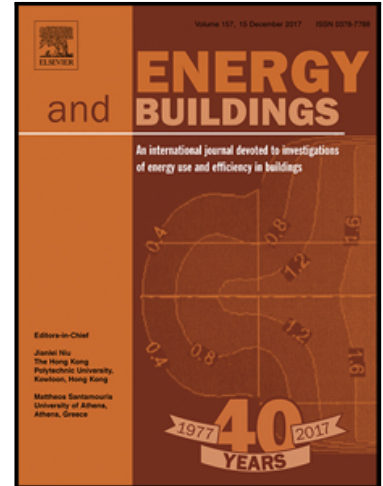


## Accepted Manuscript

Numerical Study of a Regenerative Counter Flow Evaporative Cooler using Alumina Nanoparticles in Wet Channel

Rasikh Tariq , Changhong Zhan , Xudong Zhao ,  
Nadeem Ahmed Sheikh

PII: S0378-7788(17)32764-0  
DOI: [10.1016/j.enbuild.2018.03.086](https://doi.org/10.1016/j.enbuild.2018.03.086)  
Reference: ENB 8472



To appear in: *Energy & Buildings*

Received date: 13 August 2017  
Revised date: 13 February 2018  
Accepted date: 30 March 2018

Please cite this article as: Rasikh Tariq , Changhong Zhan , Xudong Zhao , Nadeem Ahmed Sheikh , Numerical Study of a Regenerative Counter Flow Evaporative Cooler using Alumina Nanoparticles in Wet Channel, *Energy & Buildings* (2018), doi: [10.1016/j.enbuild.2018.03.086](https://doi.org/10.1016/j.enbuild.2018.03.086)

This is a PDF file of an unedited manuscript that has been accepted for publication. As a service to our customers we are providing this early version of the manuscript. The manuscript will undergo copyediting, typesetting, and review of the resulting proof before it is published in its final form. Please note that during the production process errors may be discovered which could affect the content, and all legal disclaimers that apply to the journal pertain.

© 2018. This manuscript version is made available under the CC-BY-NC-ND 4.0 license <http://creativecommons.org/licenses/by-nc-nd/4.0/>

**Highlights**

- Nanoparticles of Aluminum Oxide are added in feed water of Maisotsenko HMX.
- A mathematical model is developed for the HMX incorporating nanoparticles.
- The performance of HMX is enhanced by using nanoparticles.

ACCEPTED MANUSCRIPT

# Numerical Study of a Regenerative Counter Flow Evaporative Cooler using Alumina Nanoparticles in Wet Channel

Rasikh Tariq<sup>1</sup>, Changhong Zhan<sup>2,\*</sup>, Xudong Zhao<sup>3,¥</sup>, Nadeem Ahmed Sheikh<sup>4</sup>

<sup>1</sup> Department of Mechanical Engineering, Faculty of Engineering and Technology, HITEC University, Taxila 47080, Pakistan

<sup>2</sup> School of Architecture, Heilongjiang Cold Climate Architectural Science Key Laboratory, Harbin Institute of Technology, 66 Xidazhi Street, Harbin 150001, China

<sup>3</sup> School of Engineering and Computer Science, University of Hull, Hull HU178XH, UK

<sup>4</sup> Department of Mechanical Engineering, Faculty of Engineering and Technology, International Islamic University, Islamabad 44000, Pakistan

\* Correspondent: zhan.changhong@hit.edu.cn (C.Z.); Tel: +86-451-8628-6336; Fax: +86-451-8628-6338

¥ Co-correspondent: xudong.zhao@hull.ac.uk (X.Z.); Tel: +44-116-257-7971; +86-451-8628-6336; Fax: +44-116-257-7981

## Abstract

The use of Maisotsenko Cycle (M-Cycle) has enhanced the domain of evaporative cooling technologies to sub-wet bulb temperature cooling while ensuring moisture control. Several studies have demonstrated the use of cross-flow heat & mass exchanger (HMX) offers higher cooling capacity; however, it has lower cooling effectiveness and Energy Efficiency Ratio (EER). In contrast, a counter-flow (HMX) offers high cooling effectiveness with lower cooling capacity. In this paper, the performance of counter-flow HMX is enhanced by addition of alumina nanoparticles in feed water due to enhanced heat and mass transfer characteristics of nanofluids compared to original base fluid. Here, a mathematical model is formulated by incorporating the nanofluids in a selected control volume. The developed model is solved numerically on a discretized HMX length. Initially, the model is benchmarked against previously published results using water as base fluid. A comparison between HMX performance using water and alumina nanofluid is performed in terms of Performance Enhancement Ratio (PER). PER indicates 1-18% increase in cooling effectiveness, 18-43% increase in cooling capacity and 9-19% increase in EER by using alumina in water when working air temperature is increased from 20°C to 45°C. Similarly, an increase in PER is also observed by changing air velocity. Increase of 41% is observed in cooling capacity and 18% increase in EER is observed by changing particle volume fraction from 0 to 2 percent. This research identifies ways to reduce the carbon emissions of a building by increasing the energy efficiency of existing evaporative cooling technology using nanofluids.

**Keywords:** Building Cooling; Evaporative Cooler; M-Cycle; HMX; Nanoparticles;

## Nomenclature

Symbols	
A	Heat Transfer Surface Area, m <sup>2</sup>
a	Height, m
b	Width, m
$c_p$	Specific Heat of Fluid, J/kg. K
$D_h$	Hydraulic Diameter, m
d	Molecule's Diameter, m
EER	Energy Efficiency Ratio
f	Fluid Friction Factor
h	Convective Heat Transfer Coefficient, W/m <sup>2</sup> . K
$h_m$	Convective Mass Transfer Coefficient, kg.m <sup>2</sup> /s
$i_v$	Latent Heat of Evaporation, kJ/kg
$k_f$	Thermal Conductivity, W/m. K
$L_c$	Characteristics Length, m
L	Length of Fluid Channel, m
m	Mass Flow Rate of Fluid, kg/sec
Nu	Nusselt Number
PI	Performance Index Parameter
Pe	Peclet Number
$\Delta P$	Differential Pressure, Pa
Q	Flow Rate, m <sup>3</sup> /s
Re	Reynolds Number
RE	Relative Error
Sh	Sherwood Number
Sc	Schmidt Number
T	Temperature, °C
v	Velocity of the Fluid, m/s
$\dot{W}_{fan}$	Blowing Power, W
X	Distance, m
Z	Non-Dimensional Variable
$V_{BR}$	Particle Brownian Velocity, m/sec
Greek Letters	
$\alpha$	Thermal Diffusivity, m <sup>2</sup> /sec
$\varepsilon$	Effectiveness
$\xi$	Enthalpy, kJ/kg
$\mathcal{D}$	Mass Diffusivity, m <sup>2</sup> /sec
$\omega$	Absolute Humidity, g/kg
$\mu$	Dynamic Viscosity, N.s/m <sup>2</sup>

$\zeta$	Water Evaporation Rate, liter/hr
$\rho$	Density, kg/m <sup>3</sup>
$\nu$	Kinematic Viscosity, m <sup>2</sup> /sec
$\Gamma$	Cooling Capacity, W
$\phi$	Volume Fraction of Nanofluid
$\lambda_w$	Mean Free Path of Fluid Molecules, nm
<b>Subscript</b>	
<i>a</i>	Air
<i>dry</i>	Dry Channel
<i>DB</i>	Dry Bulb
<i>DP</i>	Dew Point
<i>Exp</i>	Experimental
<i>in</i>	Inlet
<i>m</i>	Mass Transfer
<i>NO</i>	Nanoparticle
<i>out</i>	Outlet
<i>p</i>	Product Air
<i>s</i>	Saturated
<i>Sim</i>	Numerically Simulated
<i>wet</i>	Wet Channel
<i>WB</i>	Wet Bulb
<i>w</i>	Water
<i>wa</i>	Working Air
<b>Superscript</b>	
*	Dimensionless Variable

## 1 Introduction

Building cooling requirements contribute extensively towards the world total energy consumption [1], [2]. The perspective of environmentalists for the use of green/renewable energy to overcome building cooling requirement has led the researchers and industrialist to shift towards evaporative cooling owing to its lower carbon foot print. However, evaporative cooling has few technical barriers especially while handling large cooling loads [3]. Wet bulb temperature can be achieved, at max, by utilization of only latent energy through evaporation. Moreover, direct evaporative cooling techniques increase absolute humidity and can cause discomfort for the occupants. While indirect evaporative cooling does offer solution for this but at the cost of lower cooling capacity.

The recent structural modification [4] in an indirect evaporative cooler adopting the benefits of the Maisotsenko Cycle (M-Cycle) has enabled to achieve a sub-wet bulb temperature of the air while ensuring humidity control benefits. Several other modifications [5]–[9] are presented in the structural design and flow directions to improve the effectiveness, coefficient of performance

and cooling capacity of heat and mass exchanger incorporating M-Cycle. Typically, there are two types of configuration namely; counter-flow and cross-flow HMX.

Several studies have shown numerical as well as experimental working of counter-flow [6], [8], [10], [11], cross-flow [12]–[16] and mixed flow HMX[17], [18]. Zhao et al. [8] numerically studied a counter-flow HMX and reported on the performance of HMX by varying channel air velocity, channel height, and feed water temperature. Anisimov [13] investigated the performance of cross-flow HMX by changing the parameters including inlet air conditions, and volume flow rates. Few researches focused on operational and geometric aspects [19], while some showed the performance of M Cycle for different air conditioning applications [20], [21].

Several studies have performed a comparative study of different configurations of HMX. In this regard, Zhan et al. [22] presented a detailed comparative study between a counter and a cross-flow HMX. The performance study is conducted based on product air temperature, cooling effectiveness, COP, and cooling capacity of both HMX under different operation and geometric conditions. Anisimov [23] also conducted a comparative study for different configurations of HMX. They concluded that a counter-flow HMX offers higher cooling effectiveness but lower cooling capacity compared to cross flow HMX. This merits a possible area for further investigation to improve the HMX design or properties of working fluid to improve the effectiveness as well as cooling capacity of HMX. For the crossflow configuration, Pendelidis [5] recently proposed an improved design of HMX for better cooling effectiveness. Here, an attempt is conducted to increase the performance parameters of a typical counter-flow HMX by using the nanofluid in the feed water.

Convection is a dominant mode of heat transfer in the wet channel of the HMX; therefore, the thermal conductivity of water plays a significant role in heat transfer as it directly influences the Nusselt number. It is a common observation that the thermal conductivity of liquids is comparatively less than solids [24], [25] because of the high molecular gap in liquids as compared to solids. Nanoparticles can be used to modify the thermal properties of the base fluid [26]–[28] (water) inside the HMX to enhance heat transfer properties. Several experimental and numerical researches [29]–[36] are conducted which shows that the fluid containing suspended nanoparticles manifest enhanced heat transfer properties relative to the pure working fluid. There are many combinations of nanoparticles available in the literature [37] including Alumina ( $\text{Al}_2\text{O}_3$ ),  $\text{TiO}_2$ , SiC, Fe, Cu, CuO, and Ag particles. Water and Alumina are the most common base fluid/nanoparticle combination owing to their availability, cost-effectiveness and preparation method [38]–[41]. The heat transfer properties of the water-alumina fluid-solid composite exhibit strong dependence on thermal conductivity [31], [42]–[44], particle size [45]–[47], particle volume fraction [48], [49], viscosity [50]–[53], and particle Brownian motion [54]–[60]. Several applications have demonstrated their practical usefulness such as Colangelo et al. [61] presented the contribution of the nanofluids in electronic cooling devices. Jaafar et al. [62] analyzed the heat transfer using alumina in base fluid water at different concentrations of

nanoparticles. They reported that increasing the concentration of nanoparticles is beneficial for heat transfer coefficient. Mojarrad et al. [63] experimentally investigated the heat transfer characteristics of alumina-water nanofluid for laminar flow conditions. They concluded that Nusselt number is a function of particle volume fraction and Reynolds number for a nanofluid.

In this work, the numerical performance of the HMX employing nanoparticles of alumina in the wet channel is investigated. A mathematical model is developed by applying mass and energy balances on the HMX incorporating nanofluids. The modified thermal conductivity, thermal diffusivity, mass diffusivity, and viscosity are used for the calculations of heat transfer coefficient in the wet channel considering nanoparticle size, volume fraction, and particles Brownian motion. The governing equations are simulated using Matlab [64] after the accomplishment of a convergence study for grid/mesh independence test. The results are validated initially and subsequently a parametric study is conducted based on the performance parameters of the HMX including cooling effectiveness, EER, and cooling capacity. For the parametric study, variations in ambient temperature, air velocity, and nanoparticle volume fraction are made.

## 2 System Description

A M-cycle based HMX using aluminum oxide ( $\text{Al}_2\text{O}_3$ ) nanofluid in feed water is shown in Figure 1. It is actually a modified counter-flow regenerative HMX [65] and has alternative dry and wet channels, as shown. Such a type of HMX is also analyzed by many other researchers [8], [22], [23], [65]–[67], however, in this paper, nanoparticles are added in the base fluid (water) for the purpose of heat transfer enhancement.

The product air is directly utilized for cooling purposes. While, ambient working air enters the dry channel of the HMX and is drawn to the wet channel through a porous media in the entire length of the HMX. The working air in the wet channel absorbs heat from both of its neighboring channels.

A three-dimensional selective part of Figure 1 is shown in Figure 2 to present the clear picture of its working along with its schematic psychrometric chart representation in Figure 3. Working air at ambient conditions at state 1 undergoes sensible cooling to state 2 as shown in the psychrometric chart (Figure 3) as process 1-2. Through water evaporation, temperature of working air decreases while its humidity increases as depicted in process 2-3. Furthermore, owing to lower temperature through evaporation the working air in wet channel also absorbs energy from surrounding dry and product air channels. Resultantly its temperature as well as humidity increases. In this process, the working air tends to attain saturation conditions and leaves the HMX. This is depicted as process 3-4 in the psychrometric chart (Figure 3). Nanoparticles of alumina are added in the wet channel (water) to increase the heat transfer from the surrounding channels.



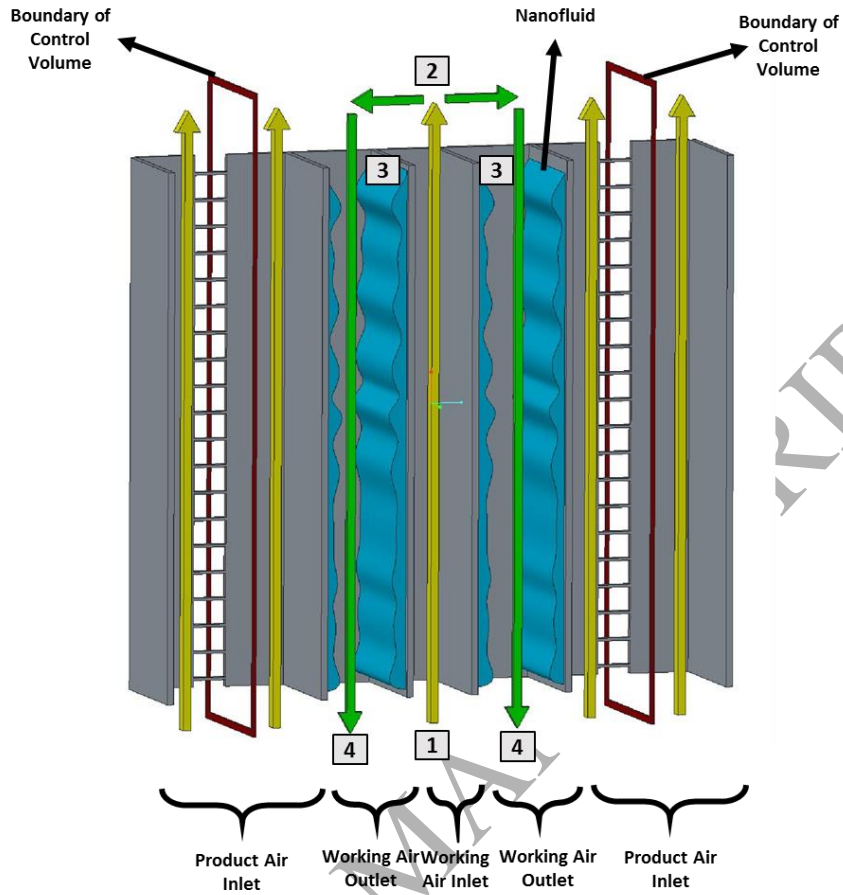


Figure 2: Three-Dimensional View of Selected Control Volume 1 for Analysis Purposes.

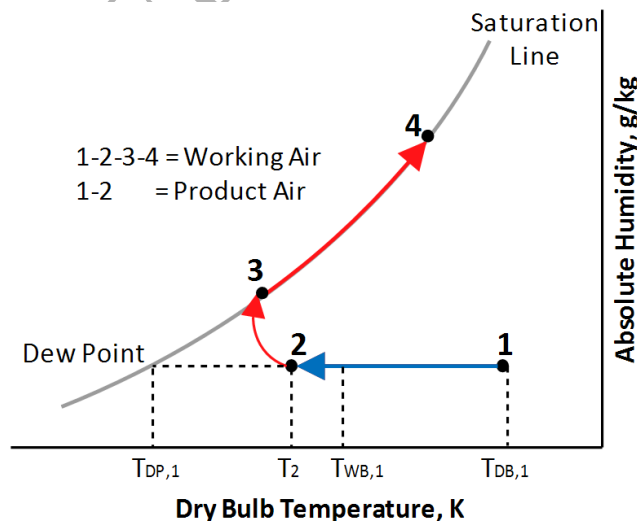


Figure 3: Psychrometric Chart of Counter-Flow Heat and Mass Exchanger (The product air is cooled to a state 2 which is below the wet-bulb temperature of state 1).

### 3 Mathematical Model

The mathematical model of this system is deduced by applying energy and mass balances at the inlet and exit of each channel. The reduction of model is carried out by considering steady-state conditions for a one-dimensional control volume having outer shells. The influence of hydrodynamic and thermal entry length is considered negligible as compared to the fully developed region, moreover, the properties of fluid are assumed to remain constant at any cross-section.

#### 3.1 Energy Balance

The mathematical model of water and nanofluid is modeled in such a fashion that the presence of nanoparticles only alters the thermal properties of water. Therefore, the governing equation is derived using water-air mixture while substituting enhanced properties of water for nanoparticles inclusion. Figure 1 shows the channels of the HMX in which Figure 1a and 1b show two different control volumes (control volume 1 and control volume 2) for the development of mathematical model as both are repetitive in the HMX. Control volume 1 is selected for analysis for the ease of computational steps. Figure 4a shows differential control volume 1 depicting the change in mass flow rate and temperature of the fluids. While, Figure 4b shows the thermal resistance diagram which shows the mode of heat transfer in control volume 1. Figure 4c lists the labels of items shown in Figure 4(a). The channels in Figure 4 are labeled as A, B, C, D and E for ease of reference.

For the product air channel, the balance of heat transfer is given by:

$$\frac{dT_p}{dx} = \frac{h_p \times b}{0.5 \times m_{p-a} \times c_{p-a}} [T_p - T_{w-Alumina}] \quad (1)$$

Multiply both sides of equation 1 by the length of the channel (L), and introduce the non-dimensional terms including:  $x^* = \frac{x}{L}$ ;  $Z_p^* = \frac{h_p \times b \times L}{0.5 \times c_{p-a} \times m_{p-a}}$ . Now, the temperature distribution in

product air can be rewritten as follows:

$$\frac{dT_p}{dx^*} = Z_p^* (T_p - T_{w-Alumina}) \quad (2)$$



Using Fick's Law, mass transfer during evaporation in wet channel can be described as:

$$dm_w = h_{m-wa-wet} (2 \times dx \times b) (\omega_{s-wet} - \omega_{wa-wet}) \quad (4)$$

Using  $x^* = \frac{x}{L}$ ;  $Z_{m-wa-wet} = \frac{h_{m-wa-wet} \times b \times L}{m_{wa}}$  and by rearranging produces:

$$\frac{d\omega_{wa-wet}}{dx^*} = 2 \times Z_{m-wa-wet} (\omega_{s-wet} - \omega_{wa-wet}) \quad (5)$$

The temperature variation for the working air in the wet channel is dependent on heat gain and latent heat of evaporation from both adjacent sides having nanofluid as shown in equation 7.

$$\begin{aligned} 0.5m_{wa} c_{p-a} T_{wa-wet} &= h_{wa-wet} (dx \times b) (T_{w-Alu\ min\ a} - T_{wa-wet}) \\ &+ h_{wa-wet} (dx \times b) (T_{w-Alu\ min\ a} - T_{wa-wet}) \\ &+ h_{m-wa-wet} (dx \times b) i_v (\omega_{s-wet} - \omega_{wa-wet}) \\ &+ h_{m-wa-wet} (dx \times b) i_v (\omega_{s-wet} - \omega_{wa-wet}) \end{aligned} \quad (6)$$

Rearranging equation 7, multiplying by the length of the channel on both sides, and introducing

the terms:  $x^* = \frac{x}{L}$ ;  $Z_{wa-wet}^* = \frac{h_{wa-wet} \times b \times L}{m_{wa} c_{p-a}}$ ;  $Z_{m-wa-wet} = \frac{h_{m-wa-wet} \times b \times L}{m_{wa}}$ , it becomes:

$$\frac{dT_{wa-wet}}{dx^*} = Z_{wa-wet}^* (T_{w-Alu\ min\ a} - T_{wa-wet}) + Z_{m-wa-wet} \frac{i_v}{c_{p-a}} (\omega_{s-wet} - \omega_{wa-wet}) \quad (7)$$

One may observe from equations 2, 4, 6, and 8 are a strong function of the thermophysical properties of the water, therefore, altering their properties using nanofluid can greatly influence the results of these equations.

There is a total of four unknowns ( $T_p, T_{wa-dry}, T_{wa-wet}, \omega_{wa-wet}$ ) described using Equations 2, 4, 6, and 8. For these first order ordinary differential equations, four boundary conditions are identified in Table 1.

Table 1: Suitable Boundary Conditions for Solution of Governing Equations

No.	Parameter	Boundary Condition
1	Product Air Inlet Temperature ( $x=0$ )	$T_{(x=0)} = T_{p,inlet}$
2	Product Air Inlet Absolute Humidity ( $x=0$ )	$\omega_{(x=0)} = \omega_{p,inlet}$
3	Working Air Dry Channel Inlet Temperature ( $x=0$ )	$T_{(x=0)} = T_{wa-dry,inlet}$
4	Working Air Dry Channel Inlet Absolute Humidity ( $x=0$ )	$\omega_{(x=0)} = \omega_{wa-dry,inlet}$

### 3.2 Supplementary Parameters

Sieder and Tate correlation [68] is used to find out the convective heat transfer coefficient ( $h$ ) of the air in the dry channel.

$$Nu = 1.86 \left( \frac{Re \times Pr}{L/D} \right)^{\frac{1}{3}} \left( \frac{\mu}{\mu_s} \right)^{0.14} = \frac{hL_c}{k_f} \quad (8)$$

The correlation used to find Sherwood number is given by [69]:

$$Sh = 0.023 Re^{0.83} Sc^{1/3} = \frac{h_{m-wa-wet} L_c}{k_f} \quad (9)$$

The properties of the nanoparticles in the wet channel are accounted in the mathematical model by using the appropriate correlation of Nusselt number, thermal diffusivity, thermal conductivity, specific heat, density and mass diffusivity. For this purpose; the mass diffusivity term ( $D_{wa-w-Alumina}$ ) appearing in the Schmidt Number ( $Sc = \nu / D_{wa-w-Alumina}$ ) is calculated which is a mixture of three substances now; water, alumina, and air. The mass diffusivity of water-alumina fluid is given by [70]:  $D_{w-Alumina} = (1-\phi)D_w$ . The modified mass diffusivity of water is calculated using [71]:  $D_{wa-w-Alumina} = 21.2 \times 10^{-6} [1 + (0.0071 \times T_{wa})]$  to find the combined diffusivity of combined mixture.

The convective heat transfer coefficient of water-alumina nanofluid is given by the following correlation [72] of Nusselt number:

$$Nu_{w-Alumina} = 0.006 \times Re_{w-Alumina}^{0.924} Pr_{w-Alumina}^{0.4} (1 + 7.6 Pe^{0.001} \phi^{0.6886}) = \frac{h_{w-Alumina} \times L_c}{k_{f-w-Alumina}} \quad (10)$$

Peclet number is calculated using [73]:  $Pe\# = u \times D_h / \alpha_{w-Alumina}$ . The thermal diffusivity of nanofluid is calculated using [72], [74]:  $\alpha_{w-Alumina} = \frac{k_{w-Alumina}}{(1-\phi)(\rho_w c_{p-w})_w + \phi(\rho_{Alumina} c_{p-Alumina})_{Alumina}}$ .

Chon [75] proposed a correlation (equation 12) which suggest that the thermal conductivity of a nanofluid depends on nanoparticle volume fraction, nanoparticle size, shape, thermo-physical properties of both substances, and the nanoparticle Brownian motion in the base fluid. Several other researches [76]–[79] also stressed on all of these aforementioned parameters.

$$\frac{k_{w-Alumina}}{k_w} = 1 + 64.7 \phi^{0.75} \left( \frac{d_w}{d_{Alumina}} \right)^{0.37} \left( \frac{k_{Alumina}}{k_w} \right)^{0.75} Pr_{w-Alumina}^{0.1} Re_{w-Alumina}^{1.2321} \quad (11)$$

The Reynolds number appearing in this equation is calculated using flow considered over one nanoparticle using the Brownian velocity [75]  $\left( V_{BR} = \frac{\kappa_B T_w}{3\pi\mu_w d_{Alumina} \lambda_w} \right)$  as follows:

$$Re\#_{w-Alumina} = \frac{\rho_w V_{BR} d_{Alumina}}{\mu_w}.$$

The specific heat ( $c_{p,w-Alumina}$ ) and density of nanofluid are calculated by employing the nanoparticle volume fraction using:  $c_{p,w-Alumina} = \phi c_{p,Alumina} + (1-\phi)c_{p-w}$  [80] and  $\rho_{w-Alumina} = \phi\rho_{Alumina} + (1-\phi)\rho_w$  [80] respectively. All the equations presented in section 3.2 exhibit that the heat and mass transfer properties of a nanofluid are strongly dependent on size, shape, concentration, and material of nanoparticle.

The water evaporation rate ( $\zeta$ ) is calculated by the difference of absolute humidity at the inlet and outlet of the working air in the wet channel as:

$$\zeta = \frac{\rho_a}{\rho_{w-Alumina}} (\omega_{wa-wet,out} - \omega_{wa-wet,in}) Q_{wa} \times 1000 \times 3600 \quad (12)$$

### 3.3 Performance Parameters

Three main performance parameters including cooling effectiveness, cooling capacity, and energy efficiency ratio (EER) are evaluated to compare the performance of HMX with normal water properties and with the use of a nanofluid. The cooling capacity is calculated by taking a difference of enthalpy at the inlet of working air-dry channel and the outlet of product air as follows:

$$\Gamma = m_{p-a} (\xi_{wa-dry,inlet} - \xi_{p-a,outlet}) \quad (13)$$

The EER of the system is defined as a ratio of the total cooling capacity of the system and the fan power as follows:

$$EER = 3.142 \times \Gamma / \dot{W}_{fan} \quad (14)$$

In this paper, it is assumed that the pumping losses are negligible as compared to the fan power. The input fan power is calculated for the product air flow and working air follow in terms of their pressure difference using the following equation:

$$\dot{W}_{fan} = \frac{(\Delta P_{wa} Q_{wa} + \Delta P_p Q_p) \times K}{1000 \times \eta_o \times \eta_l} \quad (15)$$

Chen et al. [81] proposed that the pressure drop in the working air channel is approximately three times of the pressure drop at the product air side. Therefore, the pressure drop at the product air

side is calculated using [82]:  $\Delta P_p = \frac{f}{Re\#_p} \times \frac{L}{D_h} \times \frac{\rho_a v_p^2}{2}$ . The Darcy friction factor is dependent on

the cross-sectional area of the HMX calculated using [18]:

$$f = 96 \left( 1 - 1.3553 \frac{b}{a} + 1.9467 \frac{b^2}{a^2} - 1.7012 \frac{b^3}{a^3} + 0.9564 \frac{b^4}{a^4} - 0.2537 \frac{b^5}{a^5} \right).$$

The wet-bulb and dew-point effectiveness are calculated from equation 17 and 18 respectively.

$$\epsilon_{WB} = \frac{T_{DBwa-dry,inlet} - T_{DBpa,outlet}}{T_{DBwa-dry,inlet} - T_{WBwa-dry,inlet}} \quad (16)$$

$$\epsilon_{DP} = \frac{T_{DBwa-dry,inlet} - T_{DBpa,outlet}}{T_{DBwa-dry,inlet} - T_{DPwa-dry,inlet}} \quad (17)$$

#### 4 Validation of Results

Equations 2, 4, 6 and 8 are converted into algebraic equations by numerically discretizing them using first-order finite difference scheme which is programmed on MATLAB. The fluid properties are taken from [83]. Heat transfer characteristics are evaluated using equation 9 and 10 in terms of Nusselt and Sherwood number. The nanofluid properties are computed from equation 11 and 12. Table 2 shows the geometric, operating and nanoparticle parameters selected for initial simulation purposes.

Table 2: Geometric, Operating and Nanoparticle Parameters.

No	Parameters	Quantity	Units
1	Working Air Inlet Dry Bulb Temperature	35	°C
2	Working Air Inlet Absolute Humidity	11.2	g/kg
3	Air Velocity	0.7	m/s
4	Product Air Flow Rate (Channel A or E)	120	m <sup>3</sup> /hour
5	Working Air Dry Channel Flow Rate (Channel C)	208	m <sup>3</sup> /hour
6	Working Air Wet Channel Flow Rate (Channel B and D)	104	m <sup>3</sup> /hour
7	Working Air Outlet to Working Air Inlet Ratio	0.46	-
8	Channel Length	0.9	m
9	Channel Width	314	mm
10	Channel Height	6	mm
11	Density of Alumina [56]	3880	kg/m <sup>3</sup>
12	Specific Heat of Alumina [56]	773	J/kg. K
13	Particle Volume Fraction	1.6	%
14	Diameter of Alumina Particles	46	nm
15	Density of Alumina [56]	3880	kg/m <sup>3</sup>
16	Thermal Conductivity of Alumina [56]	36	W/m. K

A total of 'n' number of control volumes are selected and iterated from  $i=1, 2, 3, \dots, n$ . Each control volume 'i' is iterated j times for mesh convergence and grid independence test. The convergence criteria are calculated by monitoring the relative error on temperature and absolute humidity at the outlet conditions of the working air from the wet channel which is presented in Figure 5(a) and 5(b). The convergence criteria are set to 0.001 for both temperature and absolute humidity. Equation 19 and 20 shows the formula of relative error for temperature and humidity.

$$RE_T = \frac{T_{i,j+1} - T_{i,j}}{T_{i,j}} \quad (18)$$

$$RE_\omega = \frac{\omega_{i,j+1} - \omega_{i,j}}{\omega_{i,j}} \quad (19)$$

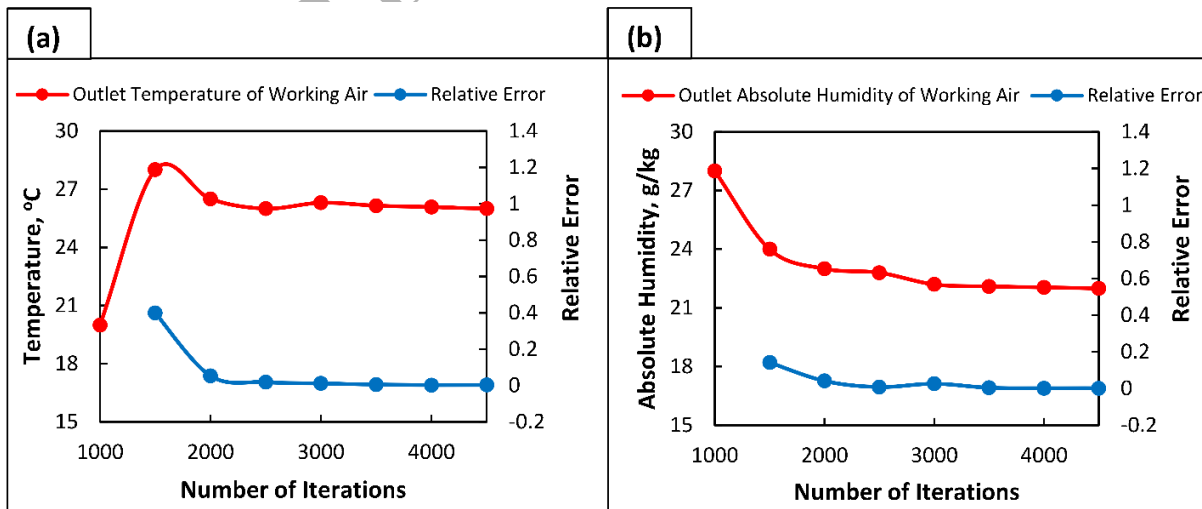


Figure 5: Grid Independence (Mesh Convergence) Study for the (a) Outlet Temperature (b) Absolute Humidity of Working Air.

The methodology diagram is descriptively shown in Figure 6 which shows the step-wise information on the developed of the code.

ACCEPTED MANUSCRIPT

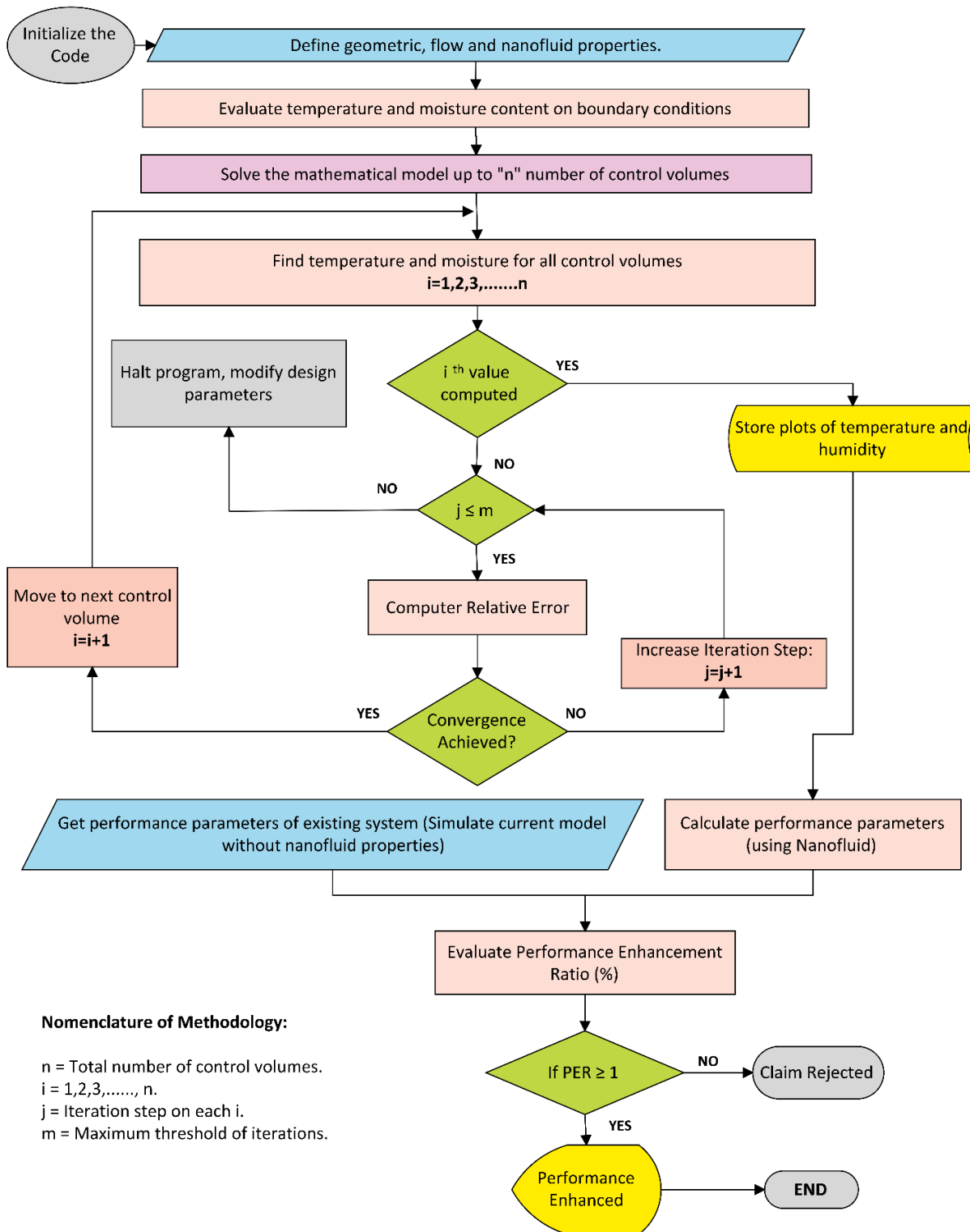


Figure 6: Methodology Diagram.

#### 4.1 Validation I

Figure 7 shows the behavior of working air without the presence of nanofluids on psychrometric chart. This analysis is performed for the validation of the mathematical model in which only water properties are used for the water. It is observed that the working air in dry channel undergoes no change in absolute humidity and it is sensibly cooled to its sub-wet bulb temperature. The working air enters into the wet passage where humidification and enthalpy addition process takes place, as a result, the temperature and the humidity of the working air increases. The exit conditions of the working air in the wet channel are compared with the conditions of Boukhanouf et al. [84]. Boukhanouf et al. [84] investigated a regenerative counter-flow HMX through experimentation and numerical simulation using normal feed water properties. A discrepancy of 1.7% is observed in the current numerical results with the findings of Boukhanouf et al. [84].

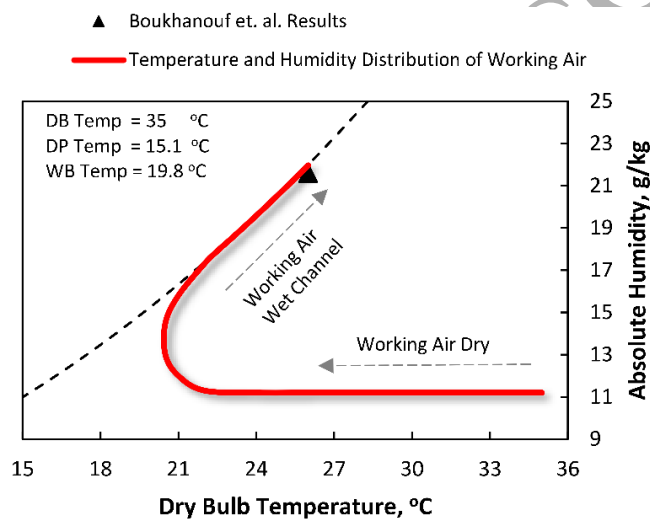


Figure 7: Behavior of Working Air in Dry Channel and Wet Channel and Point Validation with Results of Boukhanouf et al. [76]

#### 4.2 Validation II

Another validation is accomplished by a comparison with the experimental results of Duan et al. [11] who did an experimental study of a counter-flow regenerative cooler. This validation is completed using normal water properties and calculating the performance parameters by replicating the experimental conditions of Duan et al. [11] in the numerical code. Table 3 shows the comparison of both studies and a maximum percent error of 5.8% is observed in parameters.

Table 3: Validation of Numerical Results by a Comparison with Experimental Results of Duan et al. [11]

No.	Parameters	Duan et al. (2016) [11] Results	Current Simulation (With Normal Water Properties)	Percent Error (%)
1	Wet Bulb Effectiveness	1.05	1.108	5.5
2	Dew Point Effectiveness	0.78	0.825	5.8
3	Cooling Capacity, W	432	454.12	5.1
4	Energy Efficiency Ratio	10.6	11.22	5.8
5	Water Evaporation Rate, kg/hr	0.88	0.921	4.7

### 4.3 Validation III

Most of the numerical studies [10], [67], [85] conducted in the literature of counter-flow regenerative HMX are compared with the experimental results of Riangvilaikul et al. [16]. Therefore, the results of the current simulation study are also compared with the results of Riangvilaikul et al. [16] who did an experimental analysis of counter-flow regenerative HMX. This comparison is accomplished by two different simulation studies. In the first simulation study, the working air inlet temperature is varied and its influence on product air outlet temperature is observed for different humidity conditions as shown in Figure 8(a). A maximum percent error of 4.5% is observed between current simulation (with water properties) and experimental result [16]. Figure 8(b) shows the second simulation study in which the air velocity is varied from 1.5 to 6 m/s and its influence on outlet temperature of product air is reported. This study is compared with the numerical study of Lin et al. [10] and the experimental study of Riangvilaikul et al. [16]. The comparison conforms the validation of mathematical model using water properties with reported experimental results in literature.

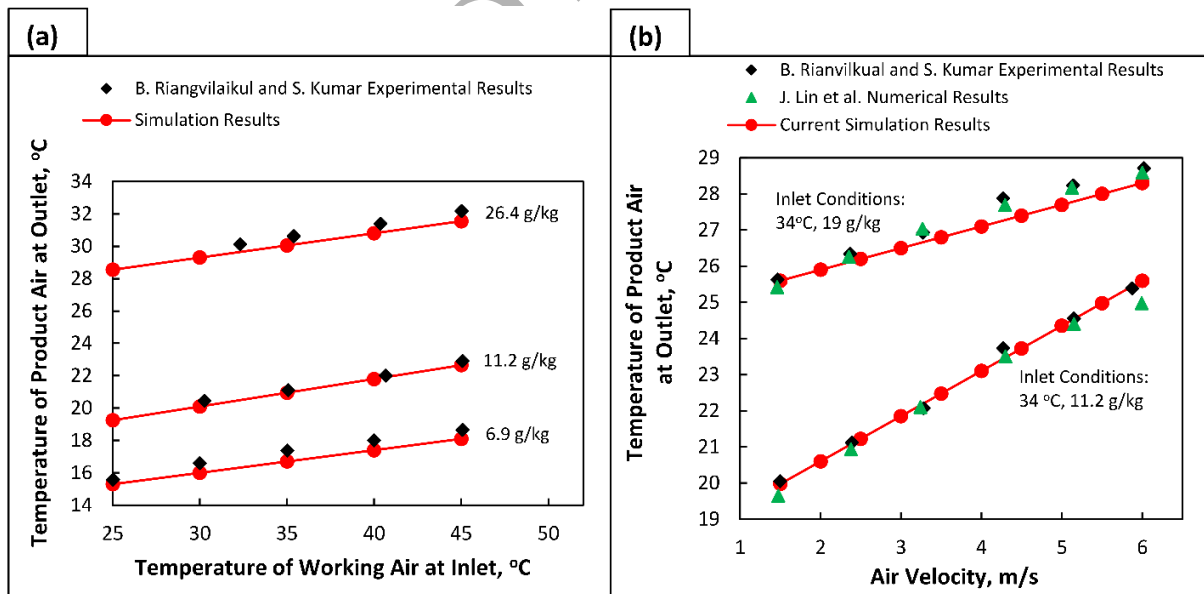


Figure 8: Validation of Numerical Results by Comparing with the Experimental Results of Riangvilaikul et al. [16] Based on (a) Temperature of Working Air at Inlet, (b) Air Velocity.

#### 4.4 Validation IV

Another comparative study is accomplished for the validation of the mathematical modeling of the pressure drop calculations in the working air channel. For this purpose, the results are compared with the findings of Lee [6] as shown in Figure 9. In this study, the volume flow rate of working air is varied from 7 to 15 m<sup>3</sup>/min for dry channel and 1.5 to 4.5 m<sup>3</sup>/min for wet channel and pressure drop is calculated for both channels. The compliance of the result shows that the pressure drop modeling of this paper is also validated.

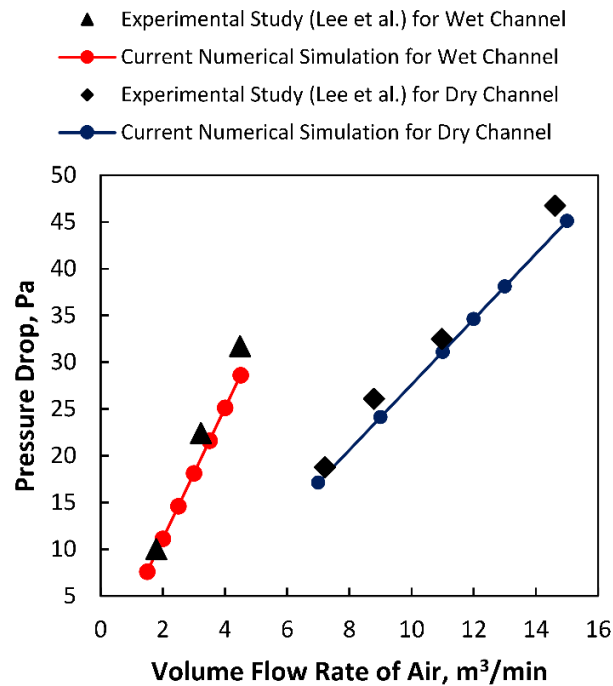


Figure 9: Validation of Pressure Drop Modelling by a Comparison with Results of Lee et al. [6]

## 5 Results and Discussions

The validation of the results, shown in previous section, is only conducted using water properties. The presented benchmarking provides confidence on the mathematical model and the solution methodology. It is important to mention that up till now no data, experimental as well numerical, can be found in the literature for use of nanofluids in M cycle based HMX. Results presented in this section are first of their kind using numerous simulations to observe the influence of the nanoparticles on the performance of the HMX.

### 5.1 Influence of Nanoparticles on Temperature and Humidity Plots

In this section, the temperature and humidity distribution equations are solved using normal water properties and nanofluid properties. The influence on the distribution is observed for both cases.

Figure 10(a) shows the temperature and humidity distribution of the product air with and without using nanoparticles. The temperature and humidity content is plotted with respect to the HMX length ratio. The product air enters at a temperature of  $35.5^{\circ}\text{C}$ . The simulation results show that the product air leaves the HMX at almost  $20^{\circ}\text{C}$  which is a sub-wet bulb temperature of this air using normal water properties. It is also observed that the supply/product air in the experimental study of Riangvilaikul et al. [16] also leaves at almost  $20.3^{\circ}\text{C}$  for similar conditions. The simulation is also conducted by using a nanofluid in the wet channel, and as a result, it is observed that the product air can achieve a temperature lower than its corresponding temperature calculated using normal water properties. This is due to the fact that the presence of nanoparticles enhances the heat transfer characteristics [28], [63], [74], and thus, it has more potential to cool the product air to be supplied to the comfort zone. The absolute humidity has no change over the length of the HMX because no moisture content is added during this process.

Figure 10(b) shows the temperature and the moisture content plot of the working air in the dry channel with and without using nanoparticles. The working air enters at a temperature of  $35.5^{\circ}\text{C}$  and leaves the HMX at  $20.3^{\circ}\text{C}$  using normal water properties. The exit conditions of working air of studies conducted by Boukhanouf et al. [84] are also justified in this numerical study using water properties. It is observed that the working air has a potential of achieving even lower temperature by using nanofluid properties instead of water [28], [63], [74]. The absolute humidity of working air in dry channel remains unchanged because of no water addition in this channel.

Figure 10(c) shows the temperature and humidity distribution of working air in the wet channel in a counter-flow configuration of HMX. The temperature and humidity of the working air at a channel length ratio of 100% is  $20.3^{\circ}\text{C}$  and  $11.2\text{ g/kg}$  which were the exit conditions of working air in the dry channel, since, the working air in the dry channel is then supplied to its adjacent wet channel. It is observed that the slope of working air employing nanofluid is steeper as compared to normal water properties because of the presence of nanofluid increases the heat transfer characteristics [63]. Similarly, the slope of humidity distribution exhibiting nanofluid properties is also steeper as compared to the humidity distribution exhibiting normal water properties because the presence of nanofluid enhances the mass transfer properties [27], [57], [74] because the presence of nanoparticles enhances the mass diffusivity and Sherwood number of the flow [70].

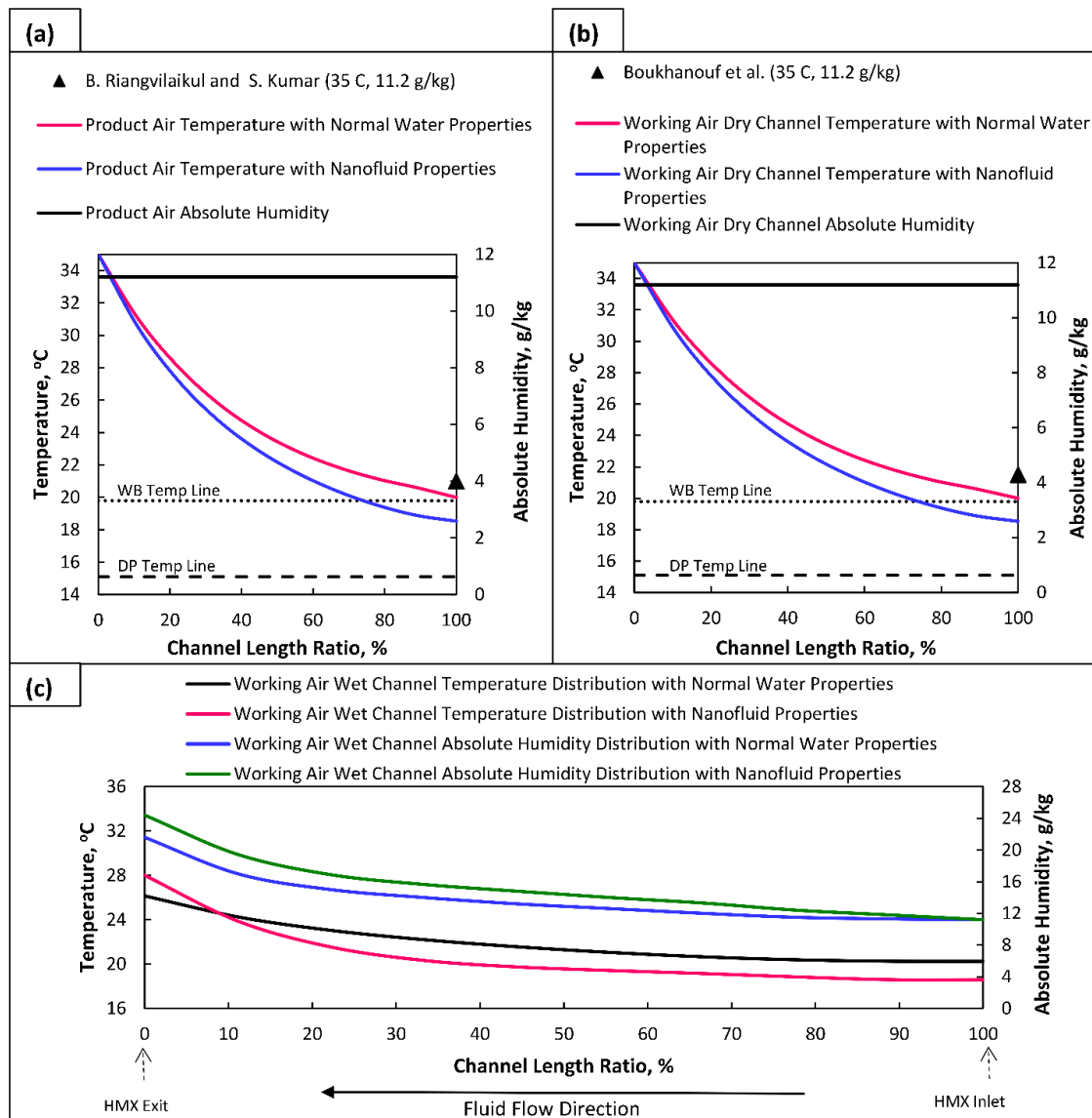


Figure 10: Temperature and Humidity Distribution in (a) Product Air Channel, (b) Working Air Dry Channel and (c) Working Air Wet Channel.

## 5.2 Influence of Working Air Inlet Temperature on Performance Parameters

In this parametric study, the inlet temperature of working air is varied from 20°C to 45°C and the performance parameters are calculated with and without using nanoparticle properties in the water.

Figure 11(a) shows the influence of working air inlet temperature on the cooling effectiveness of the HMX. It is observed that increasing the working air temperature also increases the cooling effectiveness because a high temperature has more potential to cause cooling in the wet channel, therefore, it is also expected that the cooling effectiveness can increase. It is observed that the

cooling effectiveness calculated with the presence of nanoparticles is higher as compared to normal water because of enhanced heat and mass transfer properties [27], [35], [50], [53], [58], [78]. A parameter called “Performance Enhancement Ratio” is introduced here which estimates the net increase in a performance parameter in an HMX by the addition of nanoparticles. The ratio is mathematically defined as,

$$\text{PER} = \left| \frac{\text{PI}_w - \text{PI}_{w-\text{NO}}}{\text{PI}_w} \right| \times 100 \quad (20)$$

It is observed that the PER is also increasing with increasing temperature. This is observed because at high temperature the thermal and momentum diffusivity of water-nanoparticle and air is high [31].

Figure 11(b) shows the behavior of changing working air temperature on the cooling capacity of the HMX. It is observed that the cooling capacity of the HMX is also enhanced by the addition of nanoparticles. A net increase of ~43% in the cooling capacity is observed by the addition of the nanoparticles in the water for a working air temperature of 45°C. Noting the observation of Anisimov et al. [23], the findings of this work suggest that the cooling capacity of counter-flow regenerative HMX can be increased by using the nanoparticle.

In Figure 11(c), the Energy Efficiency Ratio (EER) is plotted against the temperature of the working air. EER increases with the increase in working air temperature because for the same pumping power, the evaporation rate can be high, therefore, it gives high values of EER. It is observed that the use of nanofluid here also enhances the EER, however, the PER is not very high in this case. This is because the presence of nanoparticles increases the viscosity of the base fluid and as a result, viscous losses increases in the water feeding system, therefore, the pumping power increases too. Overall a total of ~16 increment in the EER is observed by the addition of the nanofluids for a working air temperature of 45°C.

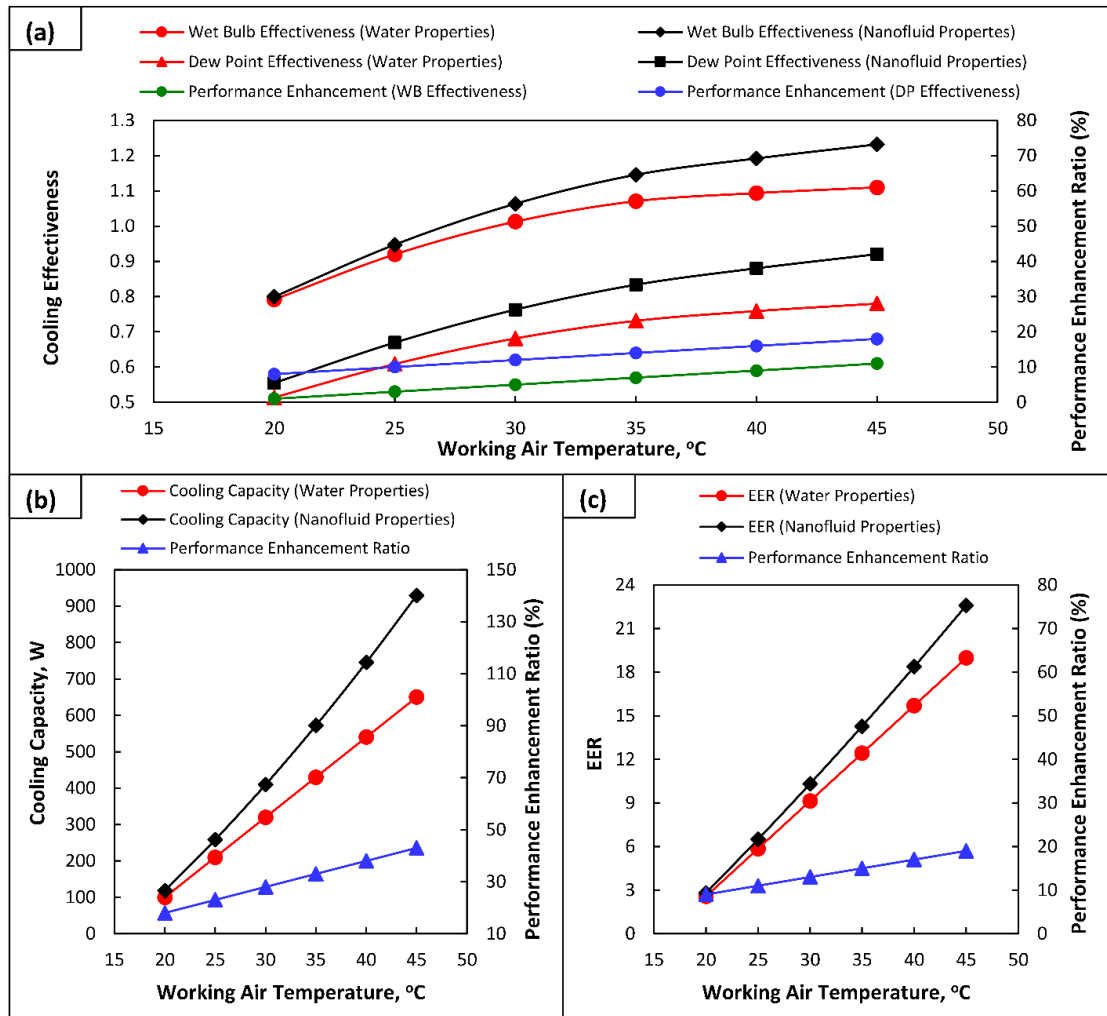


Figure 11: Effect of Working Air Inlet Temperature on the (a) Cooling Effectiveness, (b) Cooling Capacity, and (c) EER.

### 5.3 Influence of Air Velocity on Performance Parameters

Khalid et al. [7] suggested that the dew point evaporative HMX is more efficient for low-velocity conditions, therefore, in this section, lower set of air velocities (0.2 m/s to 1.6 m/s) is used to observe their influence on performance parameters.

Figure 12(a) shows the influence of air velocity on the cooling effectiveness of the HMX. It is observed that the cooling effectiveness is decreasing with the increase in air velocity because high air velocities correspond to a high-volume flow rate of air and it will give less time for the fluids to remain in contact with each other, and therefore, the cooling effectiveness is low for high velocities. The use of nanofluid enhances the cooling effectiveness as compared to normal water properties. The performance enhancement ratio is high for high air velocities because the thermal and mass diffusivity terms are high for high turbulence. A total of ~17% and ~20%

enhancement in the wet-bulb and dew-point effectiveness is observed respectively by the addition of the nanoparticles in the evaporating medium of the wet channel.

Figure 12(b) shows the behavior of cooling capacity of HMX on changing air velocities. The cooling capacity is increasing with the increase in air velocity. The presence of nanofluid further enhances the cooling capacity by ~53%, therefore, the regenerative evaporative coolers can offer high cooling capacity using nanofluids.

Figure 12(c) shows the EER with changing air velocities. The EER is decreasing with increasing air velocities because the pumping losses are dominant for high air velocities. It is observed that the presence of nanoparticles also increases the EER, however, the influence is not very significant because nanoparticles increase the viscosity of the feed water. A net total of ~22% increment is observed in the EER for an air velocity 1.6m/s.

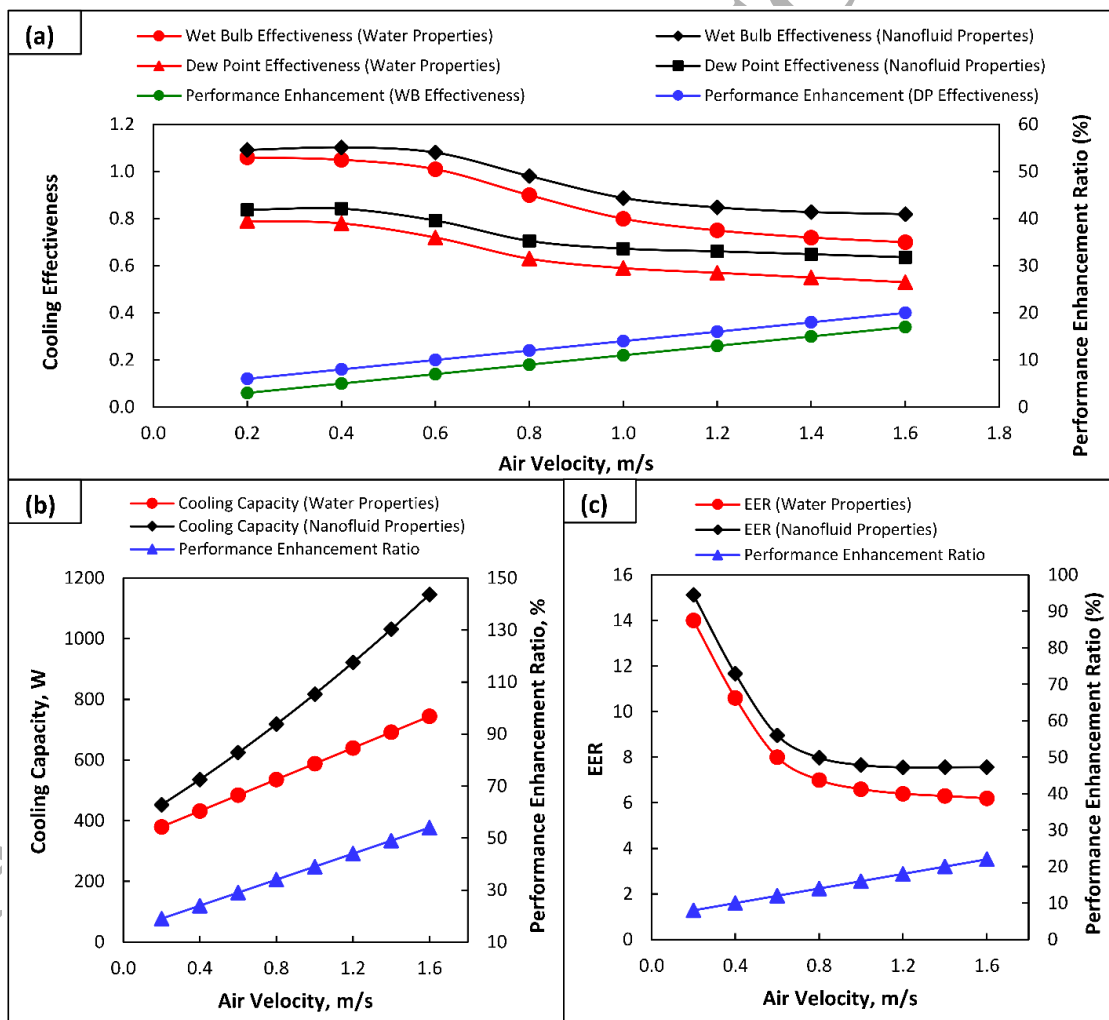


Figure 12: Influence of Air Velocity on (a) Cooling Effectiveness, (b) Cooling Capacity, and (c) Energy Efficiency Ratio.

#### 5.4 Influence of Particle Volume Fraction on Cooling Capacity and EER

The particle volume fraction is defined as the volume percentage of nanoparticles in the base fluid. Typical values of particle volume fraction are 0.4%, 1.2% and 2%. In this parametric study, the nanoparticle volume fraction is varied to observe its influence on cooling capacity and EER. Physically, the particle volume fraction corresponds to the percentage of the nanoparticles as compared to the volume fraction of the based fluid which is considered during the nanofluid preparation. It is observed from Figure 13 that cooling capacity and EER are increasing with the increase of nanoparticle volume fraction. The addition of nanoparticle enhances the thermal conductivity of the base fluid, as a result, the heat and mass transfer properties of the nanofluid are enhanced. The increase in the volume fraction of the nanoparticle enhances the heat and mass transfer characteristics, and therefore, the cooling capacity is increasing. The EER is increasing because the cooling capacity is dominant over pumping losses. Net gain of ~41% increase in cooling capacity is achieved by using volume fraction of 2% while a corresponding ~20% increase of EER is observed at the same volume fraction.

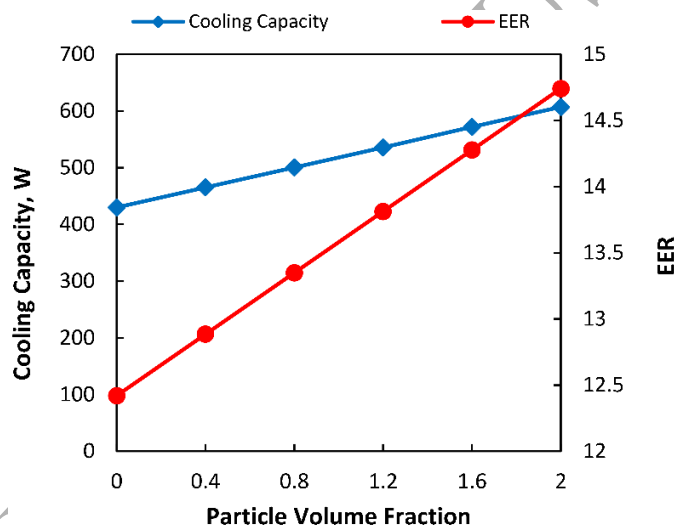


Figure 13: Influence of Particle Volume Fraction on Cooling Capacity

#### Conclusion

Maisotsenko based heat and mass exchanger (HMX) provides an energy efficient way to fulfill building cooling requirements using environment friendly technology. M cycle based cross-flow HMX offers high cooling capacity and a low cooling effectiveness; whereas, a counter-flow HMX offers high cooling effectiveness and a low cooling capacity. In this paper, the cooling capacity of a counter-flow HMX is enhanced through the use of nanoparticles of alumina in based fluid water for the wet channel. Alumina is a metallic substance which has high thermal conductivity and its presence in the water increases the heat and mass transfer characteristics of the HMX.

A mathematical model is developed and validated for the counter-flow regenerative HMX incorporating the influence of the nanoparticles. Validated is primarily carried out using water as working fluid as data for HMX using nanofluids is not available in literature. Furthermore, the influence of nanoparticle on performance parameters is observed in comparison to water. Results indicate a maximum of 18% increase in cooling capacity with 19% increase in EER at ambient temperature of 45°C. While a maximum of 54% increase in cooling capacity with 22% increase in EER are noted when air velocity is increased to 1.6 m/s. The cooling capacity is increased from 430 W to 607 W and EER is increased from 12.42 to 14.74 when the nanoparticle volume fraction is increased from 0 to 2. Finally, it is concluded that the use of nanoparticles further enhances the heat and mass transfer properties inside the wet channel, and can, therefore, lead to a sustainable and energy-efficient design of evaporative coolers. However, it is noted that the increase in concentration of nanoparticles can lead to significant viscous losses. Therefore, low concentration nanofluid is recommended for energy efficient design of evaporative air cooling applications.

## References

- [1] O. Amer, R. Boukhanouf, and H. G. Ibrahim, "A Review of Evaporative Cooling Technologies," *International J. Environ. Sci. Dev.*, vol. 6, no. 2, pp. 111–117, 2015.
- [2] L. Pérez-Lombard, J. Ortiz, and C. Pout, "A review on buildings energy consumption information," *Energy Build.*, vol. 40, no. 3, pp. 394–398, 2008.
- [3] C. Wani, S. Ghodke, and C. Shrivastava, "A review on potential of Maisotsenko cycle in energy saving applications using evaporative cooling," *Int. J. Adv. ...*, vol. 1, no. 1, pp. 15–20, 2012.
- [4] G. L., "Maisotsenko Cycle for Cooling Processes," *Clean Air*, vol. 9, no. 1–3, pp. 1–18, 2008.
- [5] D. Pandelidis, S. Anisimov, K. Rajska, E. Brychey, and M. Sidoreczyk, "Performance Comparison of The Advanced Indirect Evaporative Air," *Energy*, 2017.
- [6] J. Lee and D. Y. Lee, "Experimental study of a counter flow regenerative evaporative cooler with finned channels," *Int. J. Heat Mass Transf.*, vol. 65, pp. 173–179, 2013.
- [7] O. Khalid, M. Ali, N. A. Sheikh, H. M. Ali, and M. Shehryar, "Experimental analysis of an improved Maisotsenko cycle design under low velocity conditions," *Appl. Therm. Eng.*, vol. 95, pp. 288–295, 2016.
- [8] X. Zhao, J. M. Li, and S. B. Riffat, "Numerical study of a novel counter-flow heat and mass exchanger for dew point evaporative cooling," *Appl. Therm. Eng.*, vol. 28, no. 14–15, pp. 1942–1951, 2008.
- [9] R. Tariq and N. A. Sheikh, "Numerical heat transfer analysis of Maisotsenko Humid Air Bottoming Cycle – A study towards the optimization of the air-water mixture at bottoming turbine inlet," *Appl. Therm. Eng.*, vol. 133, no. March, pp. 49–60, 2018.
- [10] J. Lin, K. Thu, T. D. Bui, R. Z. Wang, K. C. Ng, and K. J. Chua, "Study on dew point evaporative cooling system with counter-flow configuration," *Energy Convers. Manag.*, vol. 109, pp. 153–165, 2016.
- [11] Z. Duan, C. Zhan, X. Zhao, and X. Dong, "Experimental study of a counter-flow regenerative evaporative cooler," *Build. Environ.*, vol. 104, pp. 47–58, 2016.
- [12] M. Jradi and S. Riffat, "Experimental and numerical investigation of a dew-point cooling system for thermal comfort in buildings," *Appl. Energy*, vol. 132, pp. 524–535, 2014.
- [13] S. Anisimov, D. Pandelidis, A. Jedlikowski, and V. Polushkin, "Performance investigation of a M (Maisotsenko)-cycle cross-flow heat exchanger used for indirect evaporative cooling," *Energy*, vol. 76, pp. 593–606, 2014.
- [14] D. Pandelidis and S. Anisimov, "Numerical study and optimization of the cross-flow Maisotsenko cycle indirect evaporative air cooler," *Int. J. Heat Mass Transf.*, vol. 103, pp. 1029–1041, 2016.
- [15] D. Pandelidis, S. Anisimov, W. M. Worek, and P. Drag, "Numerical analysis of a desiccant system with cross-flow Maisotsenko cycle heat and mass exchanger," *Energy Build.*, vol. 123, pp. 136–150, 2016.
- [16] B. Riangvilaikul and S. Kumar, "An experimental study of a novel dew point evaporative cooling system," *Energy Build.*, vol. 42, no. 11, pp. 637–644, 2010.

- [17] S. Moshari and G. Heidarinejad, "Numerical study of regenerative evaporative coolers for sub-wet bulb cooling with cross- and counter-flow configuration," *Appl. Therm. Eng.*, vol. 89, pp. 669–683, 2015.
- [18] H. Kim, S. Ham, D. Yoon, and J. Jeong, "Cooling performance measurement of two cross-flow indirect evaporative coolers in general and regenerative operation modes," *Appl. Energy*, vol. 195, pp. 268–277, 2017.
- [19] D. Pandelidis and S. Anisimov, "Numerical analysis of the selected operational and geometrical aspects of the M-cycle heat and mass exchanger," *Energy Build.*, vol. 87, pp. 413–424, 2015.
- [20] D. Pandelidis, S. Anisimov, and W. M. Worek, "Performance study of the Maisotsenko Cycle heat exchangers in different air-conditioning applications," *Int. J. Heat Mass Transf.*, vol. 81, pp. 207–221, 2015.
- [21] E. D. Rogdakis, I. P. Koronaki, and D. N. Tertipis, "Experimental and computational evaluation of a Maisotsenko evaporative cooler at Greek climate," *Energy Build.*, vol. 70, pp. 497–506, 2014.
- [22] C. Zhan, Z. Duan, X. Zhao, S. Smith, H. Jin, and S. Riffat, "Comparative study of the performance of the M-cycle counter-flow and cross-flow heat exchangers for indirect evaporative cooling - Paving the path toward sustainable cooling of buildings," *Energy*, vol. 36, no. 12, pp. 6790–6805, 2011.
- [23] S. Anisimov, D. Pandelidis, and J. Danielewicz, "Numerical analysis of selected evaporative exchangers with the Maisotsenko cycle," *Energy Convers. Manag.*, vol. 88, pp. 426–441, 2014.
- [24] Y. Xuan and Q. Li, "Heat transfer enhancement of nanofluids," *Int. J. heat fluid flow*, vol. 21, no. 1, pp. 58–64, 2000.
- [25] L. S. Sundar, M. H. Farooky, S. N. Sarada, and M. K. Singh, "Experimental thermal conductivity of ethylene glycol and water mixture based low volume concentration of Al<sub>2</sub>O<sub>3</sub> and CuO nanofluids," *Int. Commun. Heat Mass Transf.*, vol. 41, pp. 41–46, 2013.
- [26] H. Masuda, A. Ebata, K. Teramae, and N. Hishinuma, "Alteration of Thermal Conductivity and Viscosity of Liquid by Dispersing Ultra-Fine Particles. Dispersion of Al<sub>2</sub>O<sub>3</sub>, SiO<sub>2</sub> and TiO<sub>2</sub> Ultra-Fine Particles," *Netsu Bussei*, vol. 7, no. 4, pp. 227–233, 1993.
- [27] K. H. Solangi *et al.*, "A comprehensive review of thermo-physical properties and convective heat transfer to nanofluids," *Energy*, vol. 89, pp. 1065–1086, 2015.
- [28] S. U. S. Choi and J. A. Eastman, "Enhancing thermal conductivity of fluids with nanoparticles," in *ASME International Mechanical Engineering Congress and Exposition*, 1995, vol. 66, pp. 99–105.
- [29] H. E. Patel, S. K. Das, T. Sundararajan, A. Sreekumaran Nair, B. George, and T. Pradeep, "Thermal conductivities of naked and monolayer protected metal nanoparticle based nanofluids: Manifestation of anomalous enhancement and chemical effects," *Appl. Phys. Lett.*, vol. 83, no. 14, pp. 2931–2933, 2003.
- [30] S. M. S. Murshed, K. C. Leong, and C. Yang, "Enhanced thermal conductivity of TiO<sub>2</sub> - Water based nanofluids," *Int. J. Therm. Sci.*, vol. 44, no. 4, pp. 367–373, 2005.
- [31] H. A. Mintsa, G. Roy, C. T. Nguyen, and D. Doucet, "New temperature dependent thermal conductivity data for water-based nanofluids," *Int. J. Therm. Sci.*, vol. 48, no. 2, pp. 363–371, 2009.
- [32] W. Yu, H. Xie, L. Chen, and Y. Li, "Investigation of thermal conductivity and viscosity of ethylene glycol based ZnO nanofluid," *Thermochim. Acta*, vol. 491, no. 1–2, pp. 92–96, 2009.
- [33] Y. Hwang, H. S. Park, J. K. Lee, and W. H. Jung, "Thermal conductivity and lubrication characteristics of nanofluids," *Curr. Appl. Phys.*, vol. 6, no. SUPPL. 1, 2006.
- [34] R. S. Khedkar, S. S. Sonawane, and K. L. Wasewar, "Influence of CuO nanoparticles in enhancing the thermal conductivity of water and monoethylene glycol based nanofluids," *Int. Commun. Heat Mass Transf.*, vol. 39, no. 5, pp. 665–669, 2012.
- [35] R. V. Pinto and F. A. S. Fiorelli, "Review of the mechanisms responsible for heat transfer enhancement using nanofluids," *Applied Thermal Engineering*, vol. 108, pp. 720–739, 2016.
- [36] G. Colangelo, M. Milanese, and A. D. E. Risi, "Numerical simulation of thermal efficiency of an innovative Al<sub>2</sub>O<sub>3</sub> nanofluid solar thermal collector: influence of nanoparticles concentration," *Therm. Sci.*, pp. 1–12, 2016.
- [37] M. Milanese, F. Iacobazzi, G. Colangelo, and A. De Risi, "International Journal of Heat and Mass Transfer An investigation of layering phenomenon at the liquid – solid interface in Cu and CuO based nanofluids," *Int. J. Heat Mass Transf.*, vol. 103, pp. 564–571, 2016.
- [38] C. J. Ho, W. K. Liu, Y. S. Chang, and C. C. Lin, "Natural convection heat transfer of alumina-water nanofluid in vertical square enclosures: An experimental study," *Int. J. Therm. Sci.*, vol. 49, no. 8, pp. 1345–1353, 2010.
- [39] S. Zeinali Heris, M. Nasr Esfahany, and S. G. Etemad, "Experimental investigation of convective heat transfer of Al<sub>2</sub>O<sub>3</sub>/water nanofluid in circular tube," *Int. J. Heat Fluid Flow*, vol. 28, no. 2, pp. 203–210, 2007.

- [40] U. Rea, T. McKrell, L. wen Hu, and J. Buongiorno, "Laminar convective heat transfer and viscous pressure loss of alumina-water and zirconia-water nanofluids," *Int. J. Heat Mass Transf.*, vol. 52, no. 7–8, pp. 2042–2048, 2009.
- [41] G. Colangelo, E. Favale, P. Miglietta, M. Milanese, and A. de Risi, "Thermal conductivity, viscosity and stability of Al<sub>2</sub>O<sub>3</sub>-diathermic oil nanofluids for solar energy systems," *Energy*, vol. 95, pp. 124–136, 2016.
- [42] K. C. Leong, C. Yang, and S. M. S. Murshed, "A model for the thermal conductivity of nanofluids - The effect of interfacial layer," *J. Nanoparticle Res.*, vol. 8, no. 2, pp. 245–254, 2006.
- [43] G. Colangelo, E. Favale, A. de Risi, and D. Laforgia, "Results of experimental investigations on the heat conductivity of nanofluids based on diathermic oil for high temperature applications," *Appl. Energy*, vol. 97, pp. 828–833, 2012.
- [44] F. Jacobazzi, M. Milanese, G. Colangelo, M. Lomascolo, and A. de Risi, "An explanation of the Al<sub>2</sub>O<sub>3</sub> nanofluid thermal conductivity based on the phonon theory of liquid," *Energy*, vol. 116, pp. 786–794, 2016.
- [45] M. P. Beck, Y. Yuan, P. Warriar, and A. S. Teja, "The effect of particle size on the thermal conductivity of alumina nanofluids," *J. Nanoparticle Res.*, vol. 11, no. 5, pp. 1129–1136, 2009.
- [46] P. Warriar and A. Teja, "Effect of particle size on the thermal conductivity of nanofluids containing metallic nanoparticles," *Nanoscale Res. Lett.*, vol. 6, no. 1, p. 247, 2011.
- [47] M. Chopkar, S. Sudarshan, P. K. Das, and I. Manna, "Effect of Particle Size on Thermal Conductivity of Nanofluid," *Metall. Mater. Trans. A*, vol. 39, no. 7, pp. 1535–1542, 2008.
- [48] S. S. Khaleduzzaman, I. M. Mahbulul, I. M. Shahrul, and R. Saidur, "Effect of particle concentration, temperature and surfactant on surface tension of nanofluids," *Int. Commun. Heat Mass Transf.*, vol. 49, pp. 110–114, 2013.
- [49] B. Ravisankar and V. Tara Chand, "Influence of nanoparticle volume fraction, particle size and temperature on thermal conductivity and viscosity of nanofluids- A review," *Int. J. Automot. Mech. Eng.*, vol. 8, no. 1, pp. 1316–1338, 2013.
- [50] I. M. Mahbulul, R. Saidur, and M. A. Amalina, "Latest developments on the viscosity of nanofluids," *Int. J. Heat Mass Transf.*, vol. 55, no. 4, pp. 874–885, 2012.
- [51] F. Duan, D. Kwek, and A. Crivoi, "Viscosity affected by nanoparticle aggregation in Al<sub>2</sub>O<sub>3</sub>-water nanofluids," *Nanoscale Res. Lett.*, vol. 6, no. 1, p. 248, 2011.
- [52] L. S. Sundar, K. V. Sharma, M. T. Naik, and M. K. Singh, "Empirical and theoretical correlations on viscosity of nanofluids: A review," *Renew. Sustain. Energy Rev.*, vol. 25, pp. 670–686, 2013.
- [53] S. M. S. Murshed, K. C. Leong, and C. Yang, "Investigations of thermal conductivity and viscosity of nanofluids," *Int. J. Therm. Sci.*, vol. 47, no. 5, pp. 560–568, 2008.
- [54] J. Philip and P. D. Shima, "Thermal properties of nanofluids," *Adv. Colloid Interface Sci.*, vol. 183–184, pp. 30–45, 2012.
- [55] S. Kakac and A. Pramuanjaroenkij, "Review of convective heat transfer enhancement with nanofluids," *Int. J. Heat Mass Transf.*, vol. 52, no. 13–14, pp. 3187–3196, 2009.
- [56] V. Sridhara and L. N. Satapathy, "Al<sub>2</sub>O<sub>3</sub>-based nanofluids: a review," *Nanoscale Res. Lett.*, vol. 6, no. 1, p. 456, 2011.
- [57] S. S. Ashrafmansouri and M. Nasr Esfahany, "Mass transfer in nanofluids: A review," *Int. J. Therm. Sci.*, vol. 82, no. 1, pp. 84–90, 2014.
- [58] S. P. Jang and S. U. S. Choi, "Role of Brownian motion in the enhanced thermal conductivity of nanofluids," *Appl. Phys. Lett.*, vol. 84, no. 21, pp. 4316–4318, 2004.
- [59] Z. Haddad, E. Abu-Nada, H. F. Oztop, and A. Mataoui, "Natural convection in nanofluids: Are the thermophoresis and Brownian motion effects significant in nanofluid heat transfer enhancement?," *Int. J. Therm. Sci.*, vol. 57, pp. 152–162, 2012.
- [60] R. K. Shukla and V. K. Dhir, "Effect of Brownian Motion on Thermal Conductivity of Nanofluids," *J. Heat Transfer*, vol. 130, no. 4, p. 42406, 2008.
- [61] G. Colangelo, E. Favale, M. Milanese, A. de Risi, and D. Laforgia, "Cooling of electronic devices: Nanofluids contribution," *Applied Thermal Engineering*, vol. 127, pp. 421–435, 2017.
- [62] J. Albadr, S. Tayal, and M. Alasadi, "Heat transfer through heat exchanger using Al<sub>2</sub>O<sub>3</sub> nanofluid at different concentrations," *Case Stud. Therm. Eng.*, vol. 1, no. 1, pp. 38–44, 2013.
- [63] M. S. Mojarrad, A. Keshavarz, M. Ziabasharhagh, and M. M. Raznahan, "Experimental investigation on heat transfer enhancement of alumina/water and alumina/water-ethylene glycol nanofluids in thermally developing laminar flow," *Exp. Therm. Fluid Sci.*, vol. 53, pp. 111–118, 2014.
- [64] "MATLAB The Language of Technical Computing", 2004.
- [65] S. Anisimov and D. Pandelidis, "Numerical study of the Maisotsenko cycle heat and mass exchanger," *Int.*

- J. Heat Mass Transf.*, vol. 75, pp. 75–96, 2014.
- [66] D. Pandelidis and S. Anisimov, “Numerical analysis of the heat and mass transfer processes in selected M-Cycle heat exchangers for the dew point evaporative cooling,” *Energy Convers. Manag.*, vol. 90, pp. 62–83, 2015.
- [67] X. Cui, K. J. Chua, M. R. Islam, and W. M. Yang, “Fundamental formulation of a modified LMTD method to study indirect evaporative heat exchangers,” *Energy Convers. Manag.*, vol. 88, pp. 372–381, 2014.
- [68] E. N. Sieder and G. E. Tate, “Heat Transfer and Pressure Drop of Liquids in Tubes,” *Ind. Eng. Chem.*, vol. 28, pp. 1429–1435, 1936.
- [69] J. Welty, C. Wicks, R. Wilson, and G. Rorrer, *Fundamentals of Momentum, heat, and Mass Transfer*, vol. 1. John Wiley and Sons, 2008.
- [70] P. Singh and M. Kumar, “Mass transfer in MHD flow of alumina water nanofluid over a flat plate under slip conditions,” *Alexandria Eng. J.*, vol. 54, no. 3, pp. 383–387, 2015.
- [71] E. L. Cussler, *Diffusion: Mass Transfer in Fluid Systems*, vol. Second. Cambridge University Press, 1997.
- [72] L. I. Q. Y, “Convective heat transfer and flow characteristics of Cu-water nanofluid,” vol. 45, no. 4, 2002.
- [73] F. P. Incropera, D. P. DeWitt, T. L. Bergman, and A. S. Lavine, *Fundamentals of Heat and Mass Transfer*, vol. 7th. United States of America: John Wiley & Sons, 2007.
- [74] C. Pang, J. W. Lee, and Y. T. Kang, “Review on combined heat and mass transfer characteristics in nanofluids,” *Int. J. Therm. Sci.*, vol. 87, pp. 49–67, 2015.
- [75] C. H. Chon, K. D. Kihm, S. P. Lee, and S. U. S. Choi, “Empirical correlation finding the role of temperature and particle size for nanofluid (Al<sub>2</sub>O<sub>3</sub>) thermal conductivity enhancement,” *Appl. Phys. Lett.*, vol. 87, no. 15, p. 153107, 2005.
- [76] H. T. Zhu, C. Y. Zhang, Y. M. Tang, and J. X. Wang, “Novel Synthesis and Thermal Conductivity of CuO Nanofluid,” *J. Phys. Chem. C*, vol. 111, no. 4, pp. 1646–1650, 2007.
- [77] K. Kwak and C. Kim, “Viscosity and thermal conductivity of copper oxide nanofluid dispersed in ethylene glycol,” *Korea Australia Rheology Journal*, vol. 17, no. 2, pp. 35–40, 2005.
- [78] M. Chandrasekar, S. Suresh, and A. Chandra Bose, “Experimental investigations and theoretical determination of thermal conductivity and viscosity of Al<sub>2</sub>O<sub>3</sub>/water nanofluid,” *Exp. Therm. Fluid Sci.*, vol. 34, no. 2, pp. 210–216, 2010.
- [79] W. Evans, J. Fish, and P. Keblinski, “Role of Brownian motion hydrodynamics on nanofluid thermal conductivity,” *Appl. Phys. Lett.*, vol. 88, no. 9, 2006.
- [80] Y. Xuan and W. Roetzel, “Conceptions for heat transfer correlation of nanofluids,” *Int. J. Heat Mass Transf.*, vol. 43, no. 19, pp. 3701–3707, 2000.
- [81] Y. Chen, H. Yang, and Y. Luo, “Parameter sensitivity analysis and configuration optimization of indirect evaporative cooler (IEC) considering condensation,” *Appl. Energy*, vol. 194, pp. 440–453, 2017.
- [82] F. M. White, “Fluid Mechanics” 2009.
- [83] Moran and Shapiro, *Engineering Thermodynamics*. 2006.
- [84] R. Boukhanouf, A. Alharbi, H. G. Ibrahim, O. Amer, and M. Worall, “Computer modelling and experimental investigation of building integrated sub-wet bulb temperature evaporative cooling system,” *Appl. Therm. Eng.*, vol. 115, pp. 201–211, 2017.
- [85] D. Pandelidis, S. Anisimov, and W. M. Worek, “Comparison study of the counter-flow regenerative evaporative heat exchangers with numerical methods,” *Appl. Therm. Eng.*, 2015.